

Globally Optimized Parameters for a Model of Mitotic Control in Frog Egg Extracts

Jason W. Zwolak*, John J. Tyson**, and Layne T. Watson*+

Departments of Computer Science*, Biology**, and Mathematics+

Virginia Polytechnic Institute and State University

Blacksburg, Virginia 24061-0106

e-mail: jzwolak@vt.edu, tyson@vt.edu, ltw@vt.edu

telephone: (540) 231-5958

Abstract

DNA synthesis and nuclear division in the developing frog egg are controlled by fluctuations in the activity of M-phase promoting factor (MPF). The biochemical mechanism of MPF regulation is most easily studied in cytoplasmic extracts of frog eggs, for which careful experimental studies of the kinetics of phosphorylation and dephosphorylation of MPF and its regulators have been made. In 1998 Marlovits et al. used these data sets to estimate the kinetic rate constants in a mathematical model of the control system originally proposed by Novak and Tyson. In a recent publication, we showed that a gradient-based optimization algorithm finds a locally optimal parameter set quite close to the “Marlovits” estimates. In this paper, we combine global and local optimization strategies to show that the “refined Marlovits” parameter set, with one minor but significant modification to the Novak-Tyson equations, is the unique, best-fitting solution to the parameter estimation problem.

Keywords: global optimization, computational biology, network dynamics, ordinary differential equations, cell cycle, *Xenopus*

Abbreviations: DIRECT, dividing rectangles; ODE, ordinary differential equation; ODR, orthogonal distance regression; WSOS, weighted sum of squares

1. INTRODUCTION

The physiological attributes of a cell, its abilities to move and feed, to respond to external stimuli, to grow and reproduce, to repair damage, etc., are controlled ultimately by complex networks of interacting genes, proteins and metabolites ([1], [2]). These mechanisms can be exceedingly complex, with hundreds or thousands of interacting components [3], and ferreting out the implications of these “wiring diagrams” is beyond the scope of intuitive biochemical reasoning or reductionistic experimental data collection ([4], [5], [6]). New theoretical and computational methods are needed to make sense of the data and to gain insights into the “molecular logic” of intracellular regulatory systems ([7], [8], [9], [10]).

The gold standard of computational modeling in this domain are “bottom-up” models based on detailed biochemical kinetic descriptions of the underlying control systems, for example ([11], [12], [13], [14], [15], [16], [17], [18], [19], [20]). These models are usually framed in terms of nonlinear differential equations (ordinary, partial, or stochastic). When properly formulated, such models have distinct advantages. (1) They are closely allied to real molecular processes occurring inside cells. (2) They provide quantitatively accurate accounts of the physiological properties of cells. And (3) they can provide reliable predictions of hitherto unobserved properties of normal and mutant cells (for example, [21], [22], [23], [24]).

A major drawback of bottom-up models is that they contain many kinetic rate constants whose numerical values are unknown at the outset of the modeling exercise. The rate constants must be inferred by fitting simulations of the model to experimental observations. Parameter identification may be done by careful collection of biochemical data on component reaction steps ([16], [25]), by tedious fitting to a large collection of qualitative characteristics of cells ([12], [20]), or by rough agreement to a few crucial features of a cell’s behavior ([26], [17]). When a sufficient amount of quantitatively reliable data is available, a modeler should estimate rate constants by optimizing the goodness-of-fit of the model equations to the data.

Parameter optimization begins by defining an objective function that measures the distance between the “model” and the “data”. Generally, this distance is computed as a weighted sum of squares of distances between observed data points and corresponding simulated points. Once the objective function has been defined and computed, there are many well-tested algorithms for minimizing the function over the space of model parameters (rate constants). These algorithms are generally classified as local or global, depending on the scope of their search. Local optimization algorithms stop at the first sign of a local minimum, i.e., when the value of the objective function is lower at some point in parameter space than it is at any nearby points. Local algorithms usually work by identifying “downhill” directions in parameter space and then moving down hill as fast as possible to a local minimum. Local algorithms are computationally efficient, but they often fail to find better solutions of the optimization problem (deeper pits of the objective function) in far away regions of parameter space. Global optimization algorithms have some ability to search beyond local minima to see if better fits can be found elsewhere in parameter space. Global search algorithms generally combine an exploration step (which may be quite random or systematic) with a selection step (favoring lower values of the objective function).

We have been investigating the parameter optimization problem for a particular example of bottom-up modeling: the control of cell division in frog eggs. In Zwolak et al. [27], we used local optimization to refine a set of rate constants originally estimated by Marlovits et al. [28] by rough fitting of a mathematical model to biochemical data obtained from frog egg extracts. In this paper we apply a global optimization algorithm to show that our 2004 set of rate constants is indeed a globally optimum set of parameters. As a bonus, we find that the underlying mathematical model can be simplified somewhat, by replacing a Michaelis-Menten rate law (two kinetic parameters) with a mass-action rate law (one kinetic parameter).

2. PROBLEM DESCRIPTION

Our goal is to find an optimal parameter set for a mathematical model of the biochemistry underlying DNA synthesis and nuclear division in frog egg extracts [28]. The model (Fig. 1), proposed originally by Novak and Tyson [29], consists of a reaction network (protein species interconnected by chemical reactions) whose dynamics are cast as a set of nonlinear ordinary differential equations (ODEs). We stick with an ODE representation, because ODEs are easily simulated by computers and they accurately describe the chemical kinetics of well stirred systems. We may treat the egg extracts as well stirred because diffusion and transport occur much faster than the chemical reactions under consideration. The experimental data to be fit ([30], [31], [24], [32]) are often images of “spots” on polyacrylamide gels. The intensity of each spot represents the abundance of a particular protein species in the cell. We must estimate the relative intensity of a spot (say, 60% of maximum) in order to have numerical results for computer calculations.

2.1 Model

The reaction network in Fig. 1 can be converted into a set of ODEs for the time rates of change of the concentrations of all the proteins in the reaction mechanism. Before doing so, we make appropriate simplifications to the mechanism in Marlovits et al. [28]. All the experiments analyzed in this paper are carried out in frog egg extracts supplemented with cycloheximide, an inhibitor of protein synthesis. Hence the extract does not synthesize cyclin from its own store of cyclin mRNA, so we set $k_1 = 0$ and ignore this reaction. The experimenter adds to the extract a known amount of exogenously produced cyclin. In all cases, the added cyclin protein has been genetically engineered to be resistant to cyclosome-mediated degradation. Hence $k_2 = 0$, and we can ignore all the degradation steps in the mechanism. Because cyclin is neither synthesized nor destroyed, the total concentration of cyclin protein in the extract is constant:

$$[\text{monomeric cyclin}] + [\text{MPF}] + [\text{preMPF}] = [\text{total cyclin}] = \text{constant},$$

where MPF is the active Cdk1:cyclin dimer and preMPF refers to the phosphorylated (low activity) form of the dimer. Next, we make the assumptions (well supported by experiment) that (1) the binding of cyclin monomers and Cdk1 monomers is very fast (k_3 is large) and (2) $[\text{total Cdk1}] > [\text{total cyclin}]$. Hence $[\text{monomeric cyclin}] \ll [\text{total cyclin}]$, and the conservation condition on cyclin subunits becomes

$$[\text{MPF}] + [\text{preMPF}] = [\text{total cyclin}].$$

With these simplifications, the mechanism in Fig. 1 can be described by three ODEs

$$\frac{dM}{dt} = (v'_d(1-D) + v''_d D)(C_T - M) - (v'_w(1-W) + v''_w W)M, \quad (1)$$

$$\frac{dD}{dt} = v_d \left(\frac{M(1-D)}{K_{md} + (1-D)} - \frac{\rho_d D}{K_{mdr} + D} \right), \quad (2)$$

$$\frac{dW}{dt} = v_w \left(-\frac{MW}{K_{mw} + W} + \frac{\rho_w(1-W)}{K_{mwr} + (1-W)} \right), \quad (3)$$

where

$$\begin{aligned} M &= [\text{MPF}]/[\text{total Cdk1}], \\ D &= [\text{Cdc25P}]/[\text{total Cdc25}], \\ W &= [\text{Wee1}]/[\text{total Wee1}], \\ C_T &= [\text{total cyclin}]/[\text{total Cdk1}]. \end{aligned}$$

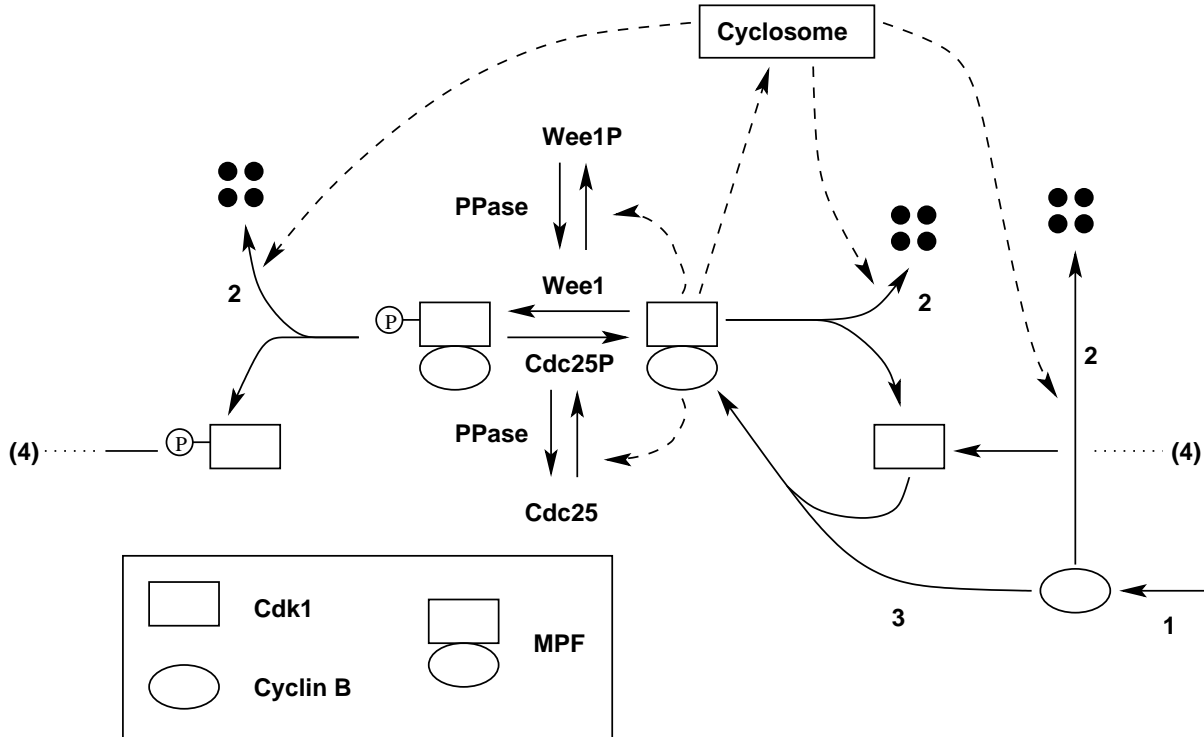


Fig. 1. The biochemical control system for MPF activation in frog egg extracts from Zwolak et al. [27]. MPF = mitosis-promoting factor = dimer of a cyclin-dependent kinase, Cdk1 (rectangle), and a B-type cyclin (oval). Rising MPF activity drives an extract through DNA synthesis, nuclear envelope breakdown, chromosome condensation, and alignment of replicated chromosomes on the mitotic spindle. Falling MPF activity allows for sister chromatid separation, nuclear reassembly, and licensing of DNA for another round of replication. Cycles of MPF activation and inactivation are driven by phases of cyclin synthesis and degradation, and by phases of Cdk1 phosphorylation (by Wee1) and dephosphorylation (by Cdc25). The newly fertilized egg has a large supply of Cdk1, the enzymes Wee1 and Cdc25, and cyclosomes (the protein complexes that promote cyclin B degradation in the steps labeled 2). The only missing component is Cyclin B. As cyclin is synthesized (step 1), it combines rapidly (step 3) with Cdk1 monomers to form active MPF dimers. The active dimers, however, are rapidly phosphorylated by Wee1 to a less active form. During this phase of the cycle, cyclins are relatively stable because the cyclosome is inactive. For the extract to enter mitosis, the inhibitory phosphate groups must be removed from Cdk1 by Cdc25. Activation of MPF is an autocatalytic process because active MPF activates Cdc25 and inhibits Wee1 (PPase is a phosphatase that opposes MPF in these reactions). As MPF activity rises, nuclei are driven into mitosis and cyclosomes are activated. The cyclosomes promote rapid cyclin degradation, which destroys MPF activity and allows nuclei to finish mitosis and prepare for a new round of DNA replication.

In Eqs. (1)–(3), time is expressed in minutes, and all concentrations are dimensionless numbers, having been scaled relative to some appropriate reference concentration. In frog egg extracts, [Cdk1] is typically close to 100 nM ([33], [24]). Total concentrations for Cdc25, Wee1 and PPase are unknown, so we set each to 1 AU (“arbitrary unit”). All v s are pseudo-first-order rate constants (units = min^{-1}). All K s are dimensionless Michaelis constants, i.e., ratios of true Michaelis constants (\bar{K} , units = concentration) to reference concentrations. The ρ s are dimensionless numbers expressing the activity of the phosphatase

(PPase, in Fig. 1) relative to MPF. The rate constants refer to the following reactions:

- v'_d — dephosphorylation of preMPF by Cdc25 in its less-active form,
- v''_d — dephosphorylation of preMPF by Cdc25 in its more-active form,
- v'_w — phosphorylation of MPF by Wee1 in its less-active form,
- v''_w — phosphorylation of MPF by Wee1 in its more-active form,
- v_d — phosphorylation of Cdc25 by MPF,
- $v_d\rho_d$ — dephosphorylation of Cdc25 by PPase,
- v_w — phosphorylation of Wee1 by MPF,
- $v_w\rho_w$ — dephosphorylation of Wee1 by PPase.

Zwolak et al. [27] describe how the parameters in Eqs. (1)–(3), the v s and K s, are related to the fundamental kinetic parameters. They also explain how to introduce a dilution factor into the calculations, because in some experiments a buffered solution of proteins is added to the frog egg extract, increasing the volume of the extract and thereby diluting all the endogenous proteins in the extract. Dilution changes the values of some of the model’s parameters from one experiment to the another, and must be taken into account when trying to fit the model to experimental observations.

2.2 Experiments

Our goal is to obtain the “best” estimates of the rate constants from the experimental data presented in Fig. 2. The figure also presents the best-fitting curves derived from Eqs. (1)–(3), using the optimal parameter values (Table 1). Experiments A–H in Fig. 2 are straightforward measurements of enzyme activity as functions of time. The data in Figs. 2I and 2J are more indirect and require further explanation.

Table 1. Selected points in parameter space used and discovered in this work. All the points were obtained by fitting the experimental data summarized in Zwolak et al. [27]. The Marlovits et al. [28] point was fit by hand. The point $\beta_{\text{LocalOnly}}$ is an optimal point obtained after local optimization was performed with $\beta_{\text{Marlovits}}$ as an initial point. β_{Global} is the result of global optimization followed by local optimization using the best point returned by the global optimizer. β_{Global3} is the result of local optimization performed on the third best point returned by the global optimizer. It is presented here for comparison to β_{Global} , as they are very similar and suggest there may be a manifold of solutions. β_{Simple} is the best point from global and local optimization on the simplified Frog Egg model with slightly different parameter names given that the model is different.

Rate Constant	$\beta_{\text{Marlovits}}$	$\beta_{\text{LocalOnly}}$	β_{Global}	β_{Global3}	β_{Simple}
v'_d	0.017	<i>0.0193</i>	0.0156	0.0153	<i>0.0152</i>
v''_d	0.17	<i>0.189</i>	0.187	0.187	<i>0.187</i>
ρ_d	0.05	0.0126	0.0013	0.0004	-
v'_w	0.01	5.1×10^{-6}	4.4×10^{-9}	7.8×10^{-7}	6.4×10^{-7}
v''_w	1.0	<i>0.986</i>	1.05	1.05	<i>1.05</i>
ρ_w	0.05	<i>0.0376</i>	0.0369	0.0366	<i>0.0366</i>
K_{md}	0.1	0.356	5.73	20.7	-
K_{mdr}	1.0	<i>0.257</i>	0.130	0.115	<i>0.111</i>
K_{mw}	0.1	<i>0.0141</i>	0.0187	0.0194	<i>0.0196</i>
K_{mwr}	1.0	<i>0.0596</i>	0.0736	0.0728	<i>0.0736</i>
v_d	2.0	5.57	44.4	152.7	-
v_w	2.0	<i>2.10</i>	2.19	2.20	<i>2.21</i>
v_{md}	-	-	-	-	7.24
v_{dr}	-	-	-	-	0.0573
$E(\beta)$	0.6001	0.03569	0.03173	0.03166	0.03165

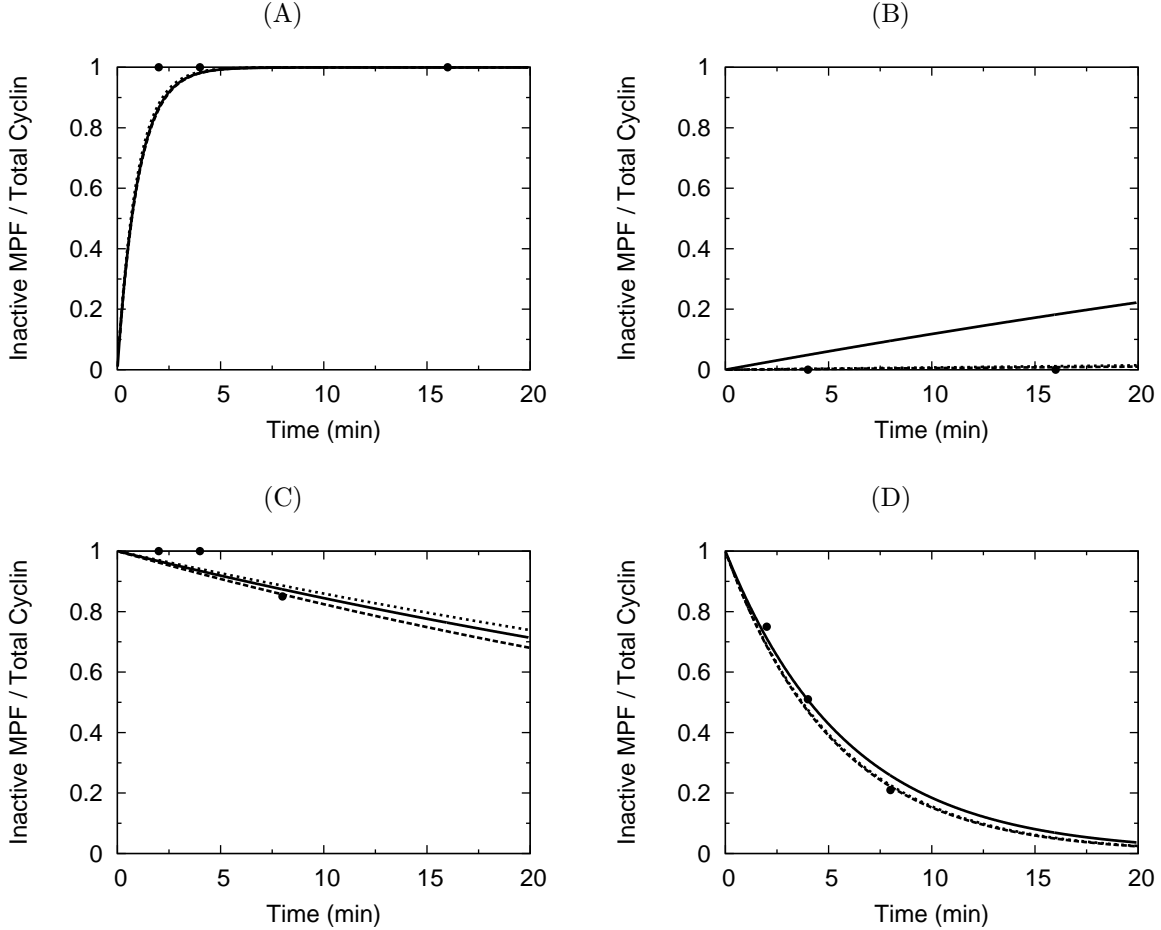


Fig. 2. Experimental data (\bullet) used for parameter estimation, simulations (\dots and $-\cdot-$) generated by the optimal points β_{Global} and $\beta_{\text{LocalOnly}}$, respectively, and simulations (—) generated by the Marlovits et al. [28] parameters. (A) Kumagai and Dunphy [31], Fig. 3C. Phosphorylation of MPF during interphase, when Wee1 is more active. (B) Kumagai and Dunphy [31], Fig. 3C. Phosphorylation of MPF during mitosis, when Wee1 is less active. (C) Kumagai and Dunphy [31], Fig. 4B. Dephosphorylation of preMPF during interphase, when Cdc25 is less active. (D) Kumagai and Dunphy [31], Fig. 4B. Dephosphorylation of preMPF during mitosis, when Cdc25 is more active. (E) Kumagai and Dunphy [30], Fig. 10A. Phosphorylation of Cdc25 during mitosis, when MPF is more active. (F) Kumagai and Dunphy [30], Fig. 10B. Dephosphorylation of Cdc25 during mitosis. (G) Tang et al. [32], Fig. 2. Phosphorylation of Wee1 during mitosis, when MPF is more active. (H) Tang et al. [32], remark in text (p. 3430). Dephosphorylation of Wee1 during interphase. (I) Moore [35]. Time lag for MPF activation. (J) Moore [35]. Thresholds for MPF activation (\uparrow) and inactivation (\downarrow).

A fundamental proposal of the Novak and Tyson [29] model of MPF oscillations in frog egg extracts is that the processes of MPF activation (dephosphorylation of preMPF by Cdc25) and MPF inactivation (phosphorylation of MPF by Wee1) are jump transitions on a hysteresis loop. To see this, we solve Eqs. (1)–(3) for the steady-state (ss) concentrations of MPF, Cdc25, and Wee1, and plot (Fig. 2J) M_{ss} as a function of C_T (total cyclin added to the extract, a parameter easily controlled by the experimentalist). The resulting system has three distinct behaviors depending on the concentration of total cyclin. The system is either stable with low MPF activity and $C_T < C_I$, stable with high MPF activity and $C_T > C_A$, or bistable with high or low MPF activity depending on whether MPF activity was initially high or low and $C_I < C_T < C_I$ ([29], [27]).

The predicted range of cyclin concentrations for which the MPF control system is bistable has recently

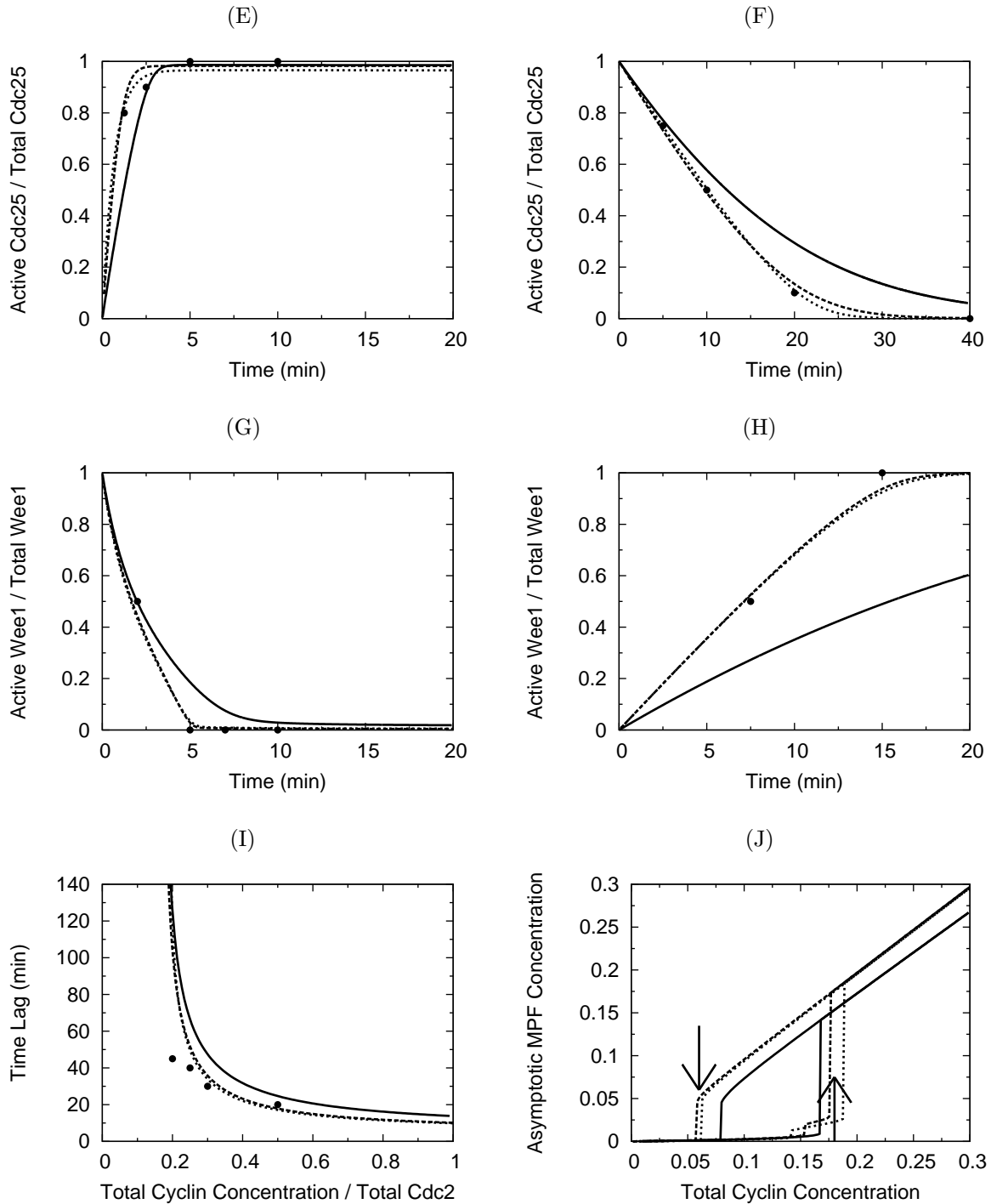


FIG. 2. Continued.

been confirmed experimentally by Sha et al. [24] and Pomerening et al. [23]. The observed range is indicated by the two arrows in Fig. 2J. The absolute amount of exogenously prepared, nondegradable cyclin that must be added to the extract at each transition point varies from one experiment to the next (e.g., 20–40 nanomol/L at the activation threshold), depending upon uncontrollable features of the procedure for preparing cyclin protein. Presumably, in some preparations, a fraction of the cyclin is inactive, so more prepared cyclin must be added to the extract to induce the transition. Comparing experiments, we find that the minimum

amount of nondegradable cyclin needed to induce MPF activation is 16nM, so we take this value as the activation threshold. In all experiments, the ratio of inactive threshold to the activation threshold is always 1/3 (regardless of their absolute magnitudes), so we take this ratio as our second experimental datum.

Novak and Tyson [29] predicted further that the time lag for activation of MPF should increase dramatically as the cyclin concentration approaches the activation threshold (16nM) from above. This prediction was confirmed by Sha et al. [24], and their data are presented in Fig. 2I.

In what follows, we shall refer to this collection of equations and experimental data as the “Xenopus model,” and attack the problem of finding a globally optimum solution to the data-fitting problem.

3. METHODS AND ALGORITHMS

Parameter estimation for problems like this is a complicated business, demanding a variety of software tools for diverse tasks and careful setup of the numerical parameters in each tool. In our case, the tasks are global optimization, local optimization, integration of stiff ODEs, and “transformation” of simulation output (e.g., MPF activity as a function of time) into the format of complex observations (e.g., MPF thresholds). The first three tasks have mature tools publicly available. The fourth task is highly specific to the scientific situation and requires specialized software. For this problem, the difficult transformations involved experiments I and J in Fig. 2. The strategy of these transformations is described in Zwolak et al. [27].

With these transformations in hand, we calculate the weighted sum of the squared differences of the calculated properties and the observed properties (Fig. 2) and provide this sum as the objective function to public domain software for numerical optimization. We use VTDIRECT [36] to perform a global search of parameter space, followed by ODRPACK [37], to refine the parameter values for our model. The model equations are integrated by LSODAR [38], a public domain software package that efficiently solves stiff and nonstiff systems of ODEs. The VTDIRECT, ODRPACK, and LSODAR codes were chosen, after consideration of many packages, for their suitability to this problem.

3.1 Objective Function

In general, a model predicts the values of dependent variables (\mathbf{y}) from independent variables (\mathbf{x}) and parameter values ($\boldsymbol{\beta}$):

$$y_i = f_i(x_i; \boldsymbol{\beta}), \quad i = 1 \dots n,$$

where \mathbf{y} , \mathbf{x} , and $\boldsymbol{\beta}$ are (in general) all vectors and f_i is the model for the i th datum. Suppose the experimental data can be expressed by vectors y_i and x_i , $i = 1, \dots, n$. If the model fits the data perfectly, for a specific parameter vector $\hat{\boldsymbol{\beta}}$, then $y_i = f_i(x_i; \hat{\boldsymbol{\beta}})$ for all i . It is always the case that there are discrepancies between the model and observations because of errors in the measurements and/or inadequacies of the model. The objective function is a scalar measure of goodness-of-fit where lower values represent a better fit of model to data. Optimizers search for parameters to minimize the objective function.

We do not assume that all measurement errors are in the dependent variables, and in fact, our model and data suggest error in the independent variable exists. For example, when the threshold for MPF activation in the model is greater than any of the time lag data points the error in the dependent variable, time, is infinite. This occurs even if the data point is close to the timelag curve in the independent variable, total cyclin concentration. For reactions such as this we seek to minimize the weighted sum of squares (WSOS) of the orthogonal distances between the model and the data:

$$E_{min} = \min_{\boldsymbol{\beta}, \boldsymbol{\delta}} \left(\sum_{i=1}^n w_{\epsilon_i} \epsilon_i^2 + w_{\delta_i} \delta_i^2 \right), \quad (4)$$

subject to the constraints

$$\epsilon_i = f_i(x_i + \delta_i; \boldsymbol{\beta}) - y_i, \quad i = 1, \dots, n. \quad (5)$$

In Eq. (4), ϵ_i and δ_i are the residuals for the dependent and independent variables, respectively, and w_{δ_i} and w_{ϵ_i} are weights for the errors. The weights are used to translate all observables into a common “currency” and to express the user’s confidence in the reliability of different observations. The solution of problem

(4)–(5) consists of $\tilde{\beta}$, $\tilde{\delta}$, $\tilde{\epsilon}$, E_{min} , giving the optimal parameter vector, the minimal discrepancies between model and observations, and a scalar measure of the overall goodness-of-fit. Convergence to the minimum solution $\tilde{\beta}$, $\tilde{\delta}$, $\tilde{\epsilon}$, and E_{min} is achieved by adjusting β and δ , where δ is treated like β —as an independent unknown.

We suggest weights of the form

$$w_{\epsilon_i} = \frac{\alpha_i}{1 + y_i^2}, \quad w_{\delta_i} = \frac{\alpha_i}{1 + x_i^2},$$

where α_i is a dimensionless number that assigns a relative importance to the i th data vector. The terms x_i^2 and y_i^2 in the denominator make the squared residuals relative and the addition of 1 ensures that experimental data close to zero will not increase the weights to unreasonably high values. In our case, we choose $\alpha_i = 1$ for all data except the thresholds. For the thresholds we choose $\alpha_i = 3$ because these two data points are actually estimated from many separate observations, and thus should be given more significance in the optimization procedure.

3.2 VTDIRECT

VTDIRECT ([36], [39], [40]) implements the DIRECT algorithm described in Jones et al. [41] and outlined here. The algorithm divides the search space (a p -dimensional box, assuming β is a p -vector) into boxes and systematically subdivides the boxes in search of regions of parameter space where the objective function values are small. The algorithm is deterministic, globally convergent, and (in a certain sense) computationally efficient. VTDIRECT calls a user-supplied objective function to evaluate points in the search space. Only these function evaluations are used; VTDIRECT does not use derivative information. Multiple points in parameter space are returned as potentially optimal with one point having the best value of the objective function.

The algorithm operates on a list of boxes and objective function values calculated at the center of each box. Initially there is a single box, encompassing the region of parameter space to be searched. In the main loop, the algorithm decides which boxes from its list to subdivide, divides them into smaller boxes, evaluates E at the center of each new box, adds the new boxes to its list, and repeats. (Note that δ and ϵ are not optimized by VTDIRECT. Instead, at each point β_i that VTDIRECT requests, the orthogonal distance (δ_i, ϵ_i) is calculated using Levenberg-Marquardt, and the WSOS is returned.) Fig. 3 illustrates how VTDIRECT might proceed on a two-dimensional parameter space after initialization, one iteration, five iterations, and ten iterations.

VTDIRECT selects boxes to be divided from its list of boxes by computing the convex hull on the lower right envelope of a scatter plot of function values versus box diameters; all boxes on the convex hull are divided. Figure 4A shows a possible scatter plot of boxes and the convex hull that VTDIRECT would compute with this scatter plot. The box diameter used in this plot is the length of the longest line that fits in the box (the line goes from a corner through the box center and to the opposite corner). VTDIRECT has a parameter ϵ that controls the bias towards exploration or convergence. ϵ 's effects can be seen graphically in Fig. 4B. Implementation aside, the role of ϵ can be understood as a fictitious box B^* inserted into the list of boxes with a diameter of 0 and a function value of $E^* := E_{min} - \epsilon|E_{min}|$, where E_{min} is the smallest function value evaluated so far. Although B^* will never be divided, it is used in the convex hull and may cause small boxes to be passed up for division on the current iteration.

The main loop continues until one of these stopping criteria are met: iteration limit, function evaluation limit, minimum box diameter tolerance, or relative change in E_{min} tolerance. VTDIRECT then returns the box B_{min} containing the parameter vector β_{min} associated with E_{min} as the best parameter values thus far. Optionally, more parameter vectors can be returned with a user-supplied minimum separation ρ . These additional vectors are selected by removing all boxes within the minimum separation distance from B_{min} , including B_{min} , then returning the next best box. Then, repeat by removing boxes within the minimum separation distance of the next best box and return a new next best box until all boxes have been removed from the box list.

We performed a few trial runs to see how fast VTDIRECT converges for our particular problem. We used these results to determine good parameters for VTDIRECT, considering that local optimization by ODRPACK would be run on each of the points returned by VTDIRECT. We used 0.001 as the tolerance for

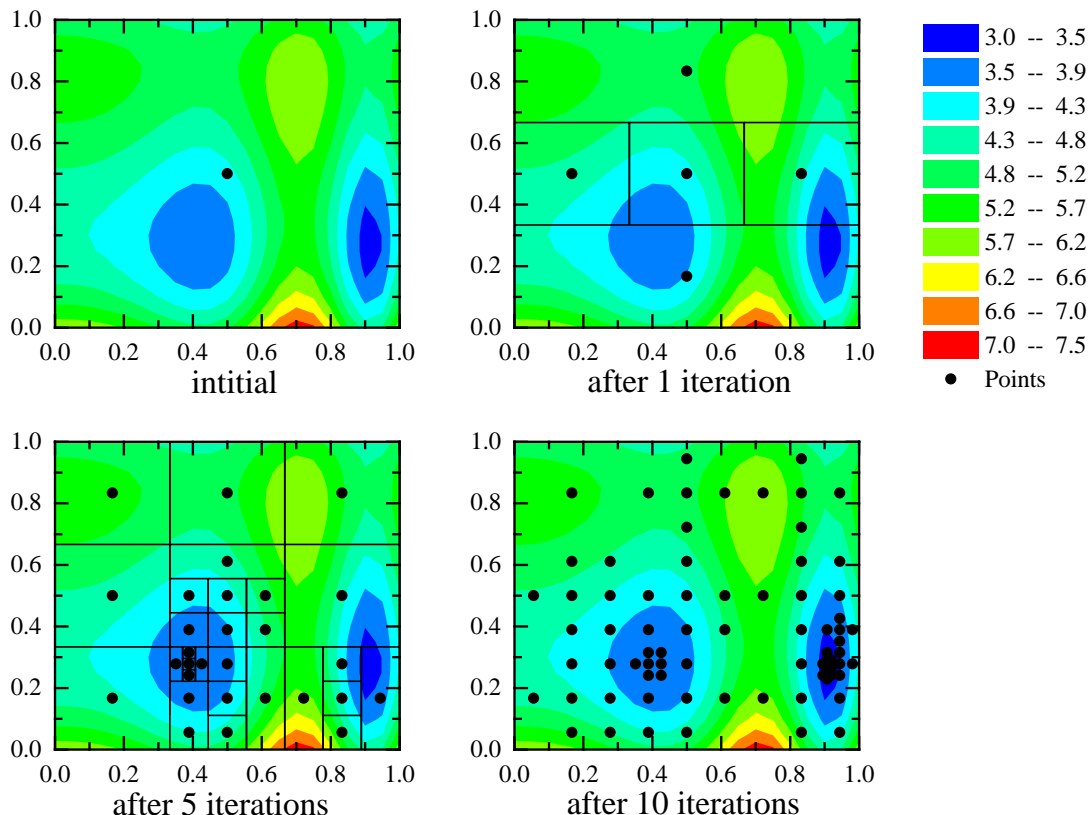


Fig. 3. A pictorial example of rectangle divisions made by VTDIRECT for a simple 2-dimensional example problem from Watson and Baker [40]. VTDIRECT quickly detects the local minimum after 5 iterations. After 10 iterations, VTDIRECT has refocused its efforts on the global minimum.

the relative change in E_{min} and left the other stopping criteria to their defaults (no limits). We used 0.01 for ϵ and $1/3$ for ρ , the minimum separation relative to the initial box diameter. For the objective function we used the same WSOS function (above) for both VTDIRECT and ODRPACK. Later we modified ϵ , ρ , and the function evaluation limit while trying to rediscover the $\beta_{LocalOnly}$ point (see the Results section).

3.3 ODRPACK

ODRPACK uses a trust region Levenberg-Marquardt method with scaling to minimize E [42]. In doing so ODRPACK needs to calculate Jacobian matrices (partial derivatives of the weighted vector (ϵ, δ) with respect to β and δ). ODRPACK can calculate these matrices by forward differences, centered differences, or by a user-supplied routine. Forward differences were used here. The default tolerances and scaling were used, and the maximum number of iterations was set to 10,000. The ODRPACK code is described in detail in Boggs et al. [43] and summarized for this problem in Zwolak et al. [27].

3.4 LSODAR

All solutions of the ODEs (1)–(3) were computed by LSODAR, a variant of LSODE ([44], [45], [38]), which automatically switches between stiff and nonstiff methods and has a root finder. LSODAR starts with a nonstiff method and switches to a stiff method if necessary. LSODAR’s root finder is used in this application to find the time lag for MPF activation. For nonstiff problems LSODAR uses Adams-Moulton (AM) of orders 1 to 12. For stiff problems LSODAR uses backward differentiation formulas (BDF) of orders 1 to 5. With both methods LSODAR varies the step size and order. LSODAR switches from AM to BDF when AM is no longer stable for the problem or cannot meet the accuracy requirements efficiently [46]. The

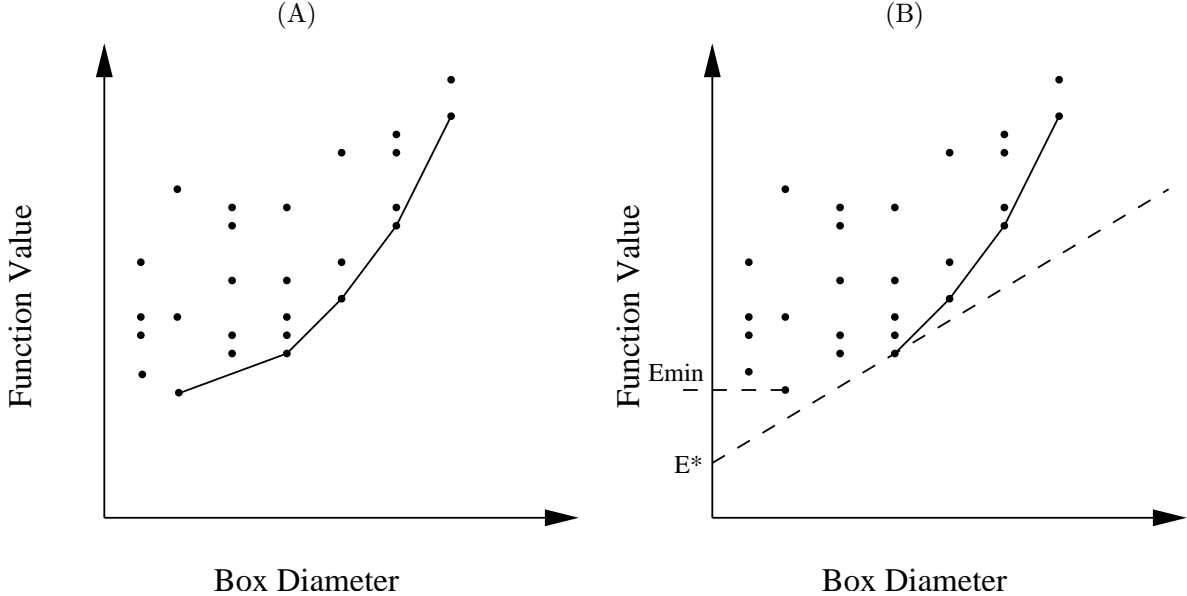


Fig. 4. These scatter plots represent a possible collection of boxes that VTDIRECT may have after some iterations. The objective function value E at the center of each box is plotted versus the box diameter (length of the longest line the box can contain). The points on the solid black line represent the boxes VTDIRECT will divide in the current iteration. (A) shows VTDIRECT’s default behavior, which is to compute the convex hull on the lower right envelope of the scatter plot. (B) shows VTDIRECT’s behavior when ϵ is set to a positive value. E^* is $E_{min} - \epsilon|E_{min}|$.

root finder in LSODAR is based on ZEROIN [47]. ZEROIN is based on code by Dekker [48]. LSODAR detects a root when the sign changes for the user-defined subroutine GEX. The tolerances are set to 10^{-10} for both relative and absolute error. A tolerance of 10^{-10} is used when calculating a root for a function of the form $M(t) - M_{root}$, where M_{root} is the value of the function $M(t)$ for which a time, t , is desired.

4. RESULTS

4.1 Global optimization of the Xenopus model

In a previous publication [27] we estimated best-fitting parameter values for the Xenopus model by local optimization, using the Marlovits et al. [28] parameters as a starting point for ODRPACK. In this paper we report on global optimization over a parameter range passed to VTDIRECT. The results of global optimization became starting points for ODRPACK to refine the parameter estimates. This strategy uncovered several local minima and the “global” minimum. The global minimum we found is different from the local minimum close to the Marlovits et al. [28] starting point. The value of the global minimum is slightly smaller (by 9%) than the value of the local minimum found in Zwolak et al. [27]. The parameters found by global optimization suggest a mathematical simplification of the model, and we recomputed the global minimum for the simplified model.

Table 2 contains the WSOS for all the initial and final points used in the parameter estimation. A baseline run was performed with $\beta_{Marlovits}$ as the initial parameters using local optimization and the computation converged to $\beta_{LocalOnly}$, which is similar to results from Zwolak et al. [27], but not identical because we are using different weights in this paper. Global parameter estimation was run with the initial range in Table 3 and a relative minimum separation of 1/3, and VTDIRECT returned four points in parameter space. Those four points were then given to the local optimizer (ODRPACK) to be refined and yielded the parameter vectors labelled β_{Global} , $\beta_{Global2}$, $\beta_{Global3}$, and $\beta_{Global4}$ in Table 2. Notice that β_{Global} is the optimal parameter set for the Xenopus model, where $\beta_{Global2}$, $\beta_{Global3}$, and $\beta_{Global4}$ are locally optimal, globally suboptimal solutions.

$\beta_{Global2}$ and $\beta_{Global4}$ were thrown out because of their high WSOS compared to β_{Global} and $\beta_{Global3}$.

Table 2. Weighted sum of squares (WSOS) of the residuals for local parameter estimation with various starting points from the global optimizer. Also included is the Marlovits et al. [28] initial guess.

Point	WSOS
$\beta_{\text{Marlovits}}$	0.60014
$\beta_{\text{LocalOnly}}$	0.0356919
β_{Global}	0.03173179
β_{Global2}	0.2515503
β_{Global3}	0.0316594
β_{Global4}	0.14134885
$\beta_{\text{GlobalContinued}}$	0.03165119
β_{Simple}	0.0316514
β_{Simple2}	0.2516655
β_{Simple3}	0.0316593

β_{Global} and β_{Global3} have similar parameter values as can be seen in Table 1. These points in parameter space were explored further.

4.2 Simplification of the *Xenopus* model

The points β_{Global} and β_{Global3} differ considerably from $\beta_{\text{LocalOnly}}$ in that the parameters K_{md} and v_d are much larger in the “global” vectors than in the “local only” vector. Two parameters characterize the Michaelis-Menten function used to describe the kinetics of Cdc25 phosphorylation by active MPF. The value of K_{md} is more than five times larger than the maximum concentration of Cdc25 (scaled to be 1). Hence, substrate concentration is always $\ll K_{md}$, and the enzyme (MPF) is operating in the linear range of its kinetic rate law. From a mathematical perspective,

$$\frac{v_d M(1-D)}{K_{md} + (1-D)}$$

becomes

$$\frac{v_d M(1-D)}{K_{md}}$$

for $K_{md} \gg (1-D)$, and then the ratio v_d/K_{md} can be simplified to a single constant v_{md} . Figure 5 demonstrates that this simplification of the rate law is entirely justified for values of inactive Cdc25 concentration in its operational range, 0–1.

The new model is

$$\frac{dM}{dt} = (v'_d(1-D) + v''_d D)(C_T - M) - (v'_w(1-W) + v''_w W)M, \quad (6)$$

$$\frac{dD}{dt} = v_{md}M(1-D) - \frac{v_{dr}D}{K_{mdr} + D}, \quad (7)$$

$$\frac{dW}{dt} = v_w \left(-\frac{MW}{K_{mw} + W} + \frac{\rho_w(1-W)}{K_{mwr} + (1-W)} \right), \quad (8)$$

with the following new parameters:

$$\begin{aligned} v_{md} & \text{— mass action rate constant, replacing } v_d/(K_{md} + (1-D)), \\ v_{dr} & \text{— dephosphorylation of Cdc25 by PPase, replacing } v_d\rho_d. \end{aligned}$$

After this simplification the points β_{Global} and β_{Global3} are seen to be the same solution: the values of (v_{md}, v_{dr}) are (7.75, 0.0074) and (7.36, 0.0079) for β_{Global} and β_{Global3} , respectively.

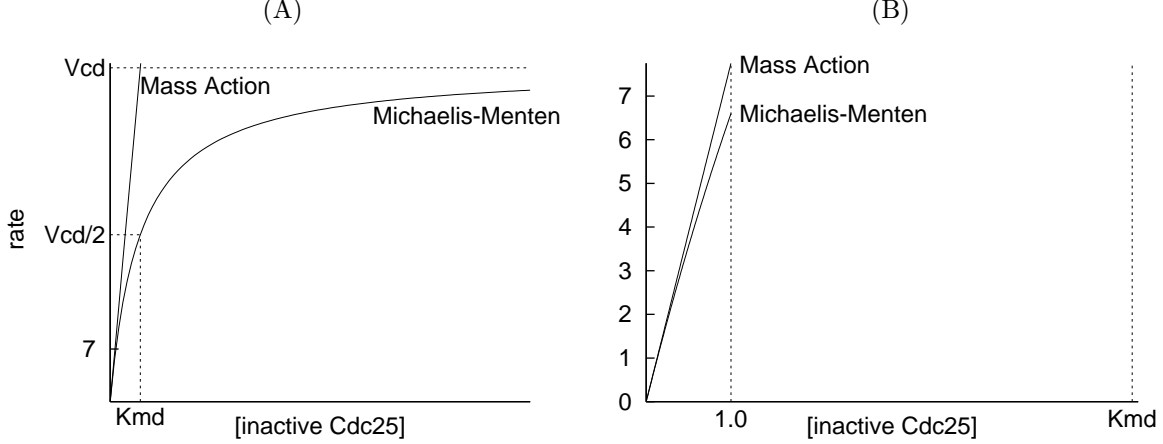


Fig. 5. The reaction rate term containing K_{md} from Eq. (2) versus inactive Cdc25 using the point β_{Global} from Table 1. (A) shows the rate of mass action kinetics and Michaelis-Menten kinetics to a range 0–80 for [inactive Cdc25]. (B) shows a blow up of (A) for values of [inactive Cdc25] from 0 to K_{md} . Here, the difference between mass action and Michaelis-Menten kinetics is insignificant for valid values of [inactive Cdc25], from 0 to 1.

Global and local parameter estimation was then performed with the new equations and parameters. First, local optimization was run with β_{Global} as the starting point. The local optimization yielded a point close to the starting point. The WSOS of this point can be seen in Table 2 as $\beta_{\text{GlobalContinued}}$. Second, global optimization was run with the same ranges specified in Table 3 and returned multiple points with relative minimum separation of 1/3, each of which was then used as the starting point for local optimization. The WSOS of the three points returned are in Table 2 labeled β_{Simple} , β_{Simple2} , and β_{Simple3} . β_{Simple2} was discarded for its high WSOS. β_{Simple} and β_{Simple3} are the same point. β_{Simple} , recorded in Table 1, is similar to β_{Global} and β_{Global3} .

Table 3. Ranges of parameters used for VTDIRECT while globally searching parameter space. The upper bounds were picked conservatively in case a better fit far from the Marlovits initial parameters exists.

Parameter	Lower	Upper
v'_d	0	1
v''_d	0	10
v'''_d	0	1
v'_w	0	1
v''_w	0	10
v'''_w	0	1
K_{md}	0	10
K_{mdr}	0	100
K_{mw}	0	10
K_{mwr}	0	100
v_d	0	100
v_w	0	100
μ	1	10

4.3 The basin of attraction of $\beta_{\text{LocalOnly}}$

We explored the parameter space further in an attempt to rediscover the solution $\beta_{\text{LocalOnly}}$. The search space was cut by a factor greater than 2^{13} , about half the size in each dimension, the ϵ parameter

to VTDIRECT was increased giving more weight towards exploration, and the stopping criterion was set to 10,000 function evaluations. Six points were returned with a relative minimum separation of $1/5$ (which is conveniently $1/2$ the distance between β_{Global} and $\beta_{\text{LocalOnly}}$). Of these points two were closer to $\beta_{\text{LocalOnly}}$ than to β_{Global} . One point was an absolute distance of 15 from $\beta_{\text{LocalOnly}}$ and 33 from β_{Global} , and the other was 30 from $\beta_{\text{LocalOnly}}$ and 40 from β_{Global} . Only the first of the two was evaluated further. Local optimization was run and it converged to β_{Global} . We could not find the point $\beta_{\text{LocalOnly}}$ with global optimization even though we used our knowledge of the location of $\beta_{\text{LocalOnly}}$ in our search. None of the points returned by the global optimizer followed by the local optimizer were close to $\beta_{\text{LocalOnly}}$. VTDIRECT explored tens of thousands of points and we expected some of the better points to fall in the basin of attraction of $\beta_{\text{LocalOnly}}$. The best points fell into the basin of attraction of β_{Global} . After removing all points around β_{Global} within the minimum separation distance the next best point fell into the basin of attraction of β_{Global2} , and similarly, the next best points fell into the basins of attraction of β_{Global3} and β_{Global4} .

Why did our attempts to find $\beta_{\text{LocalOnly}}$ fail? What properties of the objective function around $\beta_{\text{LocalOnly}}$ could explain our results? Possibly, the basin of attraction of $\beta_{\text{LocalOnly}}$ is near one of the other basins and small enough to fit within the minimum separation distance. Perhaps, the $\beta_{\text{LocalOnly}}$ basin is not small but is mostly shallow and has a steep drop off near $\beta_{\text{LocalOnly}}$. Perhaps, the $\beta_{\text{LocalOnly}}$ basin is very small in which case it may have been missed altogether by VTDIRECT. Or perhaps, the best points of the $\beta_{\text{LocalOnly}}$ basin fall within the minimum separation distance of the point returned by the global optimizer for β_{Global} , and the points outside that minimum separation distance are considerably higher than other points outside that distance.

We counted the number of points VTDIRECT evaluated around β_{Global} and around $\beta_{\text{LocalOnly}}$ within a ball of radius one half the distance between β_{Global} and $\beta_{\text{LocalOnly}}$. About 700 out of the 10,000 points from the last global optimization fell within the ball around $\beta_{\text{LocalOnly}}$, and about 3000 fell within the ball around β_{Global} . VTDIRECT was dividing boxes more heavily around β_{Global} than $\beta_{\text{LocalOnly}}$. This means there are more promising boxes near β_{Global} than $\beta_{\text{LocalOnly}}$. We can infer that the parameter space around β_{Global} has a larger range with good values of the objective function since more boxes were divided. Although not directly correlated, we conjecture that the basin of attraction for β_{Global} is in some sense larger and/or deeper than the basin of $\beta_{\text{LocalOnly}}$. $\beta_{\text{LocalOnly}}$ was obtained using $\beta_{\text{Marlovits}}$ as the starting point to ODRPACK. In support of this conjecture, we point out that $\beta_{\text{LocalOnly}}$ and $\beta_{\text{Marlovits}}$ are a distance of 3.7 apart, whereas $\beta_{\text{LocalOnly}}$ and its closest point returned by VTDIRECT are a distance of 15 apart. By comparison convergence to β_{Global} was obtained from points as far away as 80.

Figure 6 provides some views of the objective function over slices of the parameter space between several locally optimal points. The objective function was calculated in four different planes in parameter space specified by three points each. The points used are $\beta_{\text{LocalOnly}}$, β_{Global} , β_{Global2} , and β_{Global4} . (β_{Global3} is not used because it is similar to β_{Global} .) Figures 6A and 6B show that $\beta_{\text{LocalOnly}}$ and β_{Global} are in a valley together; there is not much of an increase in the objective function between them as compared to next to them (towards β_{Global2} and β_{Global4}). Furthermore, the basin of attraction of β_{Global} seems larger than that of $\beta_{\text{LocalOnly}}$ (the objective function values around β_{Global} are smaller than that of $\beta_{\text{LocalOnly}}$ given the same radius around them). Although inconclusive by itself, Fig. 6 provides evidence that β_{Global} has a larger basin of attraction with better objective function values than $\beta_{\text{LocalOnly}}$. These properties would bias VTDIRECT and ODRPACK towards β_{Global} , as we have seen in our parameter estimation runs.

5. DISCUSSION

The “bottom-up” approach to Systems Biology attempts to build accurate and realistic mathematical models of the molecular machinery underlying a certain aspect of cell physiology. These models contain many kinetic parameters (rate constants, binding constants, etc.) that must be estimated by comparing model simulations to experimental measurements. Although this procedure of estimating the kinetic parameters from the very experiments that the model is trying to explain is often criticized as being circular reasoning or vacuous curve-fitting (“with four parameters I can fit an elephant”), the fact is that all kinetic parameters are ultimately estimated, in one way or another, by fitting the consequences of kinetic rate laws to experimental data. The question is not whether the parameters are estimated from the data or not, but whether we have sufficient experimental observations both to estimate the parameters and to provide meaningful tests of the mechanism. Novak and Tyson, and their colleagues, have been studying these issues for many years on a model of DNA synthesis and nuclear division in frog eggs and frog egg extracts. In Round One, Novak and

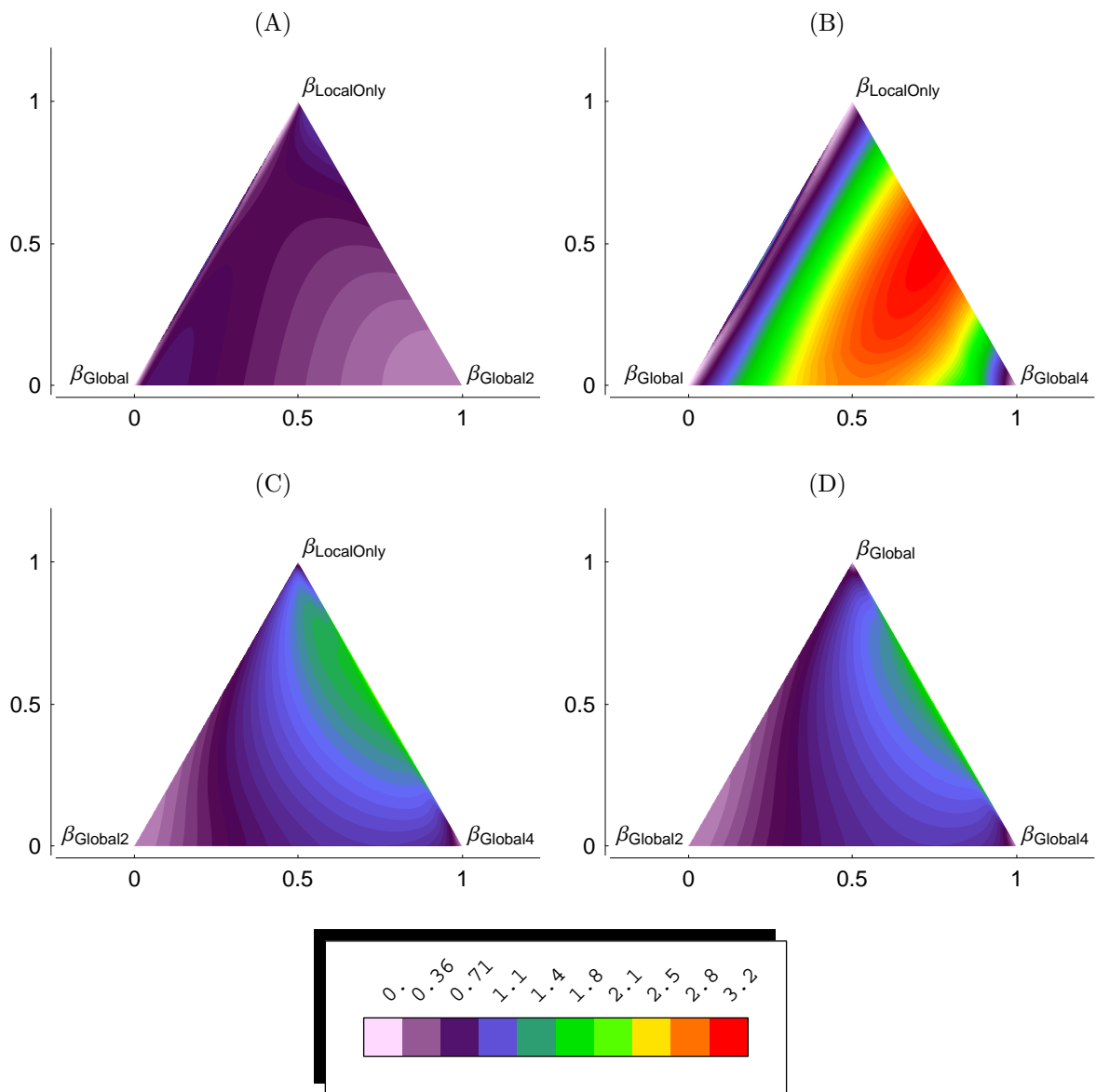


Fig. 6. Contour plots of two-dimensional cuts in parameter space between four groups of three points each. All the unique points returned by the global followed by local optimization are used from the first run of VTDIRECT. These plots provide hints why β_{Global} is repeatedly reached by our optimizers while $\beta_{\text{LocalOnly}}$ is reached only with $\beta_{\text{Marlovits}}$ as the starting point for local optimization.

Tyson [29] proposed the model and estimated the kinetic constants from a consideration only of very general qualitative features of the control system (steady states, oscillations, thresholds, etc.). They made three qualitative predictions about the control system (“hysteresis”, “slowing down”, and “checkpoint elevation”) that were confirmed ten years later [24]. In addition, in the mid 1990s, there appeared several biochemical studies ([30], [31], [35], and [32]) of rates of component reactions in the Novak-Tyson mechanism. Although these experiments were not done to test the model, their results were in surprisingly good quantitative agreement with the Novak-Tyson estimates of the kinetic constants, as shown by Marlovits et al. [28]. The latter authors did the sort of back-of-an-envelope calculations familiar to biophysical chemists, but did not try to fit the model rigorously to the data, to estimate optimal parameter values, or to characterize how deviations from the optimum affect the goodness of fit.

We addressed these issues in Zwolak et al. [27], using a local optimization algorithm [34] with the Marlovits parameter set ($\beta_{\text{Marlovits}}$) as a starting point. We found a locally optimal parameter set $\beta_{\text{LocalOnly}}$, close to $\beta_{\text{Marlovits}}$. Sampling the objective function $E(\beta)$, close to $\beta_{\text{LocalOnly}}$, we found the expected bowl-shape with some parameter combinations tightly constrained by the data and other combinations much less constrained.

In this paper we address the question whether the parameter set $\beta_{\text{LocalOnly}}$ is a globally optimal solution of the Xenopus model. To this end, we used a deterministic, global optimization procedure (“dividing rectangles”) to explore a large region of parameter space, encompassing what we consider to be all possible reasonable values of the model’s kinetic constants. The global optimizer efficiently explores this domain and returns “promising regions” of parameter space (where $E(\beta)$ is small and/or β is sufficiently far away from other promising regions). The global optimizer is not efficient at homing in on optimal points, so each promising region is studied further by the local optimizer. This procedure identified three local minima of the objective function, at points we call β_{Global} , β_{Global2} , and β_{Global4} . (β_{Global3} was deemed to be indistinguishable from β_{Global} .) These three local minimum points are all different from each other and from $\beta_{\text{LocalOnly}}$. At these points the objective function takes on the following values: $E(\beta_{\text{Global}}) = 0.032$, $E(\beta_{\text{LocalOnly}}) = 0.036$, $E(\beta_{\text{Global4}}) = 0.14$, $E(\beta_{\text{Global2}}) = 0.25$. The two best solutions, β_{Global} , and $\beta_{\text{LocalOnly}}$, give equally good fits to the data (Fig. 2), whereas the solutions β_{Global4} and β_{Global2} are less satisfactory (Fig. 7).

The major difference between β_{Global} and $\beta_{\text{LocalOnly}}$ is reflected in the kinetic rate law used to describe one step in the reaction mechanism. $\beta_{\text{LocalOnly}}$ treats this particular MPF-catalyzed reaction as a Michaelis-Menten rate law that is noticeably saturated in the operational range of substrate concentrations, whereas β_{Global} treats the reaction as operating in the linear range of substrate concentrations. This observation suggested that the model be simplified, replacing the Michaelis-Menten rate law (two kinetic constants) by a mass-action rate law (one kinetic constant). The optimal parameter set for the simplified model we call β_{Simple} .

In Table 2 we have italicized those values of the kinetic constants shared by β_{Simple} and $\beta_{\text{LocalOnly}}$. These italicized rate constants are essentially identical, given the experimental uncertainty of the data used to estimate them. In this light, we do not have two different “optimal” parameter vectors, but only one parameter vector and two slightly different models. In one model, MPF-catalyzed phosphorylation of Cdc25 is depicted as a Michaelis-Menten-type reaction, and in the other model it is described by a simpler mass-action rate law. In all other aspects, the two models are in complete agreement about rate laws and kinetic constants.

REFERENCES

- [1] Bray, D.: ‘Protein molecules as computational elements in living cells’, *Nature*, 1995, **376**, pp. 307–312
- [2] Hanahan, D., and Weinberg, R. A.: ‘The hallmarks of cancer’, *Cell*, 2000, **100**, pp. 57–70
- [3] Kohn, K. W.: ‘Molecular interaction map of the mammalian cell cycle control and DNA repair systems’, *Mol. Biol. Cell*, 1999, **10**, pp. 2703–2734
- [4] Hartwell, L. H., Hopfield, J. J., Leibler, S., and Murray, A. W.: ‘From molecular to modular cell biology’, *Nature*, 1999, **402**, pp. C47–52
- [5] Brent, R.: ‘Genomic biology’, *Cell*, 2000, **100**, pp. 169–183
- [6] Lazebnik, Y.: ‘Can a biologist fix a radio?— Or, what I learned while studying apoptosis’, *Cancer Cell*, 2002, (2), pp. 179–82
- [7] Hasty, J., Millen, D., Isaacs, F., and Collins, J. J.: ‘Computational studies of gene regulatory networks: in numero molecular biology’, *Nat. Rev. Genet.*, 2001, **2**, pp. 268–279
- [8] Tyson, J. J., Chen, K., and Novak, B.: ‘Network Dynamics and Cell Physiology’, *Nature Reviews Molecular Cell Biology*, 2001, **2**, pp. 908–16
- [9] Brazhnik, P., de la Fuente, A., and Mendes, P.: ‘Gene networks: how to put the function in genomics’, *Trends Biotechnol.*, 2002, (20), pp. 467–72
- [10] Kumar S. P., and Feidler, J. C.: ‘BioSPICE: a computational infrastructure for integrative biology’, *OMICS*, 2003, (7), pp. 225
- [11] Martiel, J. L., and Goldbeter, A.: ‘A model based on receptor desensitization for cyclic-AMP signaling in Dictyostelium cells’, *Biophys. J.*, 1987, **52**, pp. 808–828

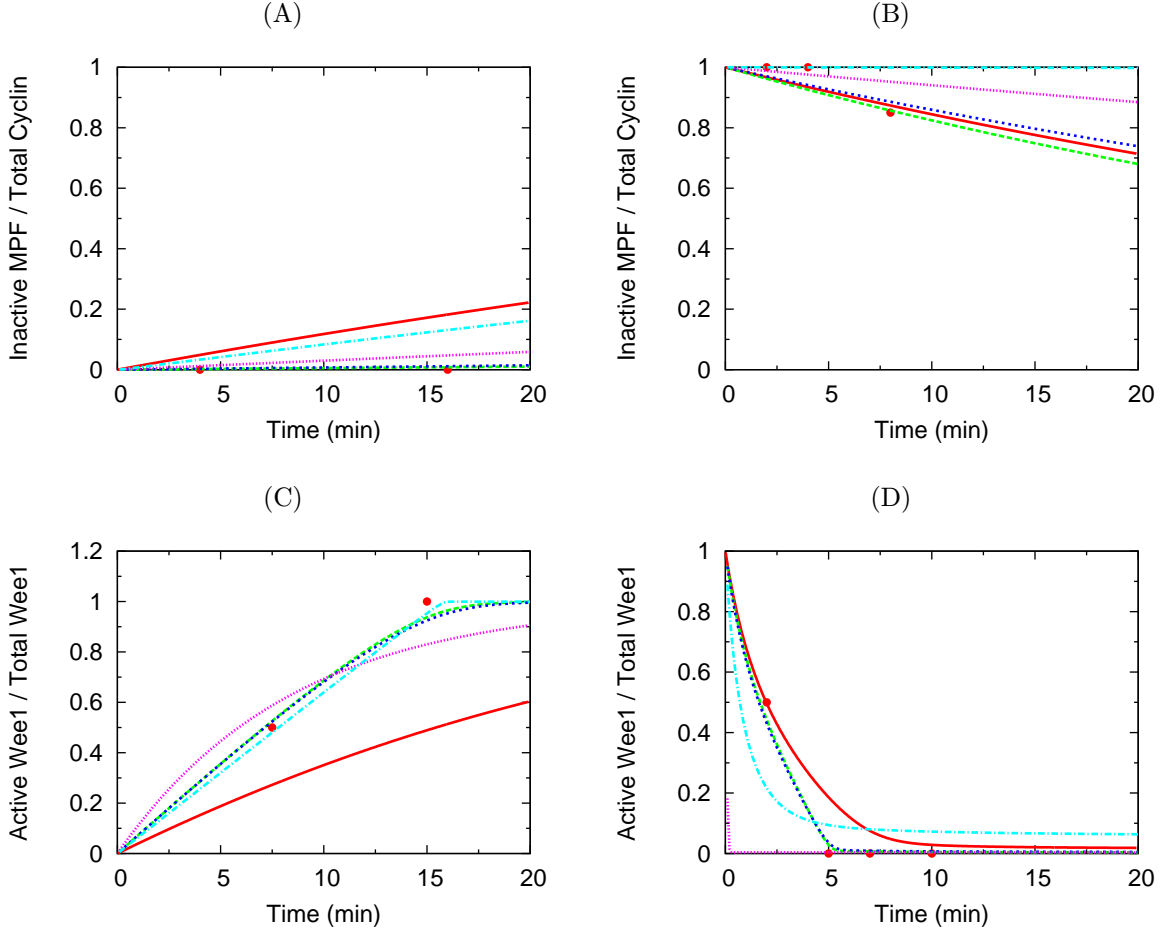


Fig. 7. Four plots showing simulations using β_{Global2} (·-·-) and β_{Global4} (-·-·-) in comparison with $\beta_{\text{Marlovits}}$ (—), $\beta_{\text{LocalOnly}}$ (- - -), and β_{Global} (- - -) from Fig. 2. The experimental data is plotted with \bullet . These plots represent the cases where β_{Global2} and β_{Global4} fail to accurately reproduce experimental data at an acceptable level for further analysis (as was performed on β_{Global}). The plots not shown give equally good fits for β_{Global2} and β_{Global4} as is seen with β_{Global} in Fig. 2.

- [12] Bray, D., Bourret, R. B., and Simon, M. I.: ‘Computer simulation of the phosphorylation cascade controlling bacterial chemotaxis’, *Mol. Biol. Cell*, 1993, **4**, (5), pp. 469–482
- [13] McAdams, H. H., and Shapiro, L.: ‘Circuit simulation of genetic networks’, *Science*, 1995, **269**, pp. 650–656
- [14] Arkin, A., Ross, J., and McAdams, H. H.: ‘Stochastic kinetic analysis of developmental pathway bifurcation in phage lambda-infected *Escherichia coli* cells’, *Genetics*, 1998, **149**, pp. 1633–1648
- [15] Sharp, D. H., and Reinitz, J.: ‘Prediction of mutant expression patterns using gene circuits’, *Biosystems*, 1998, **47**, pp. 79–90
- [16] Teusink, B., Passarge, J., Reijenga, C. A., Esgalhado, E., van der Weijden, C. C., Schepper, M., Walsh, M. C., Bakker, B. M., van Dam, Karel, Westerhoff, H. V., and Snoep, J. L.: ‘Can yeast glycolysis be understood in terms of *in vitro* kinetics of the constituent enzymes? Testing biochemistry’, *Eur. J. Biochem*, 2000, (267), pp. 5313–5329
- [17] von Dassow, G., Meir, E., Munro, E. M., and Odell, G. M.: ‘The segment polarity network is a robust developmental module’, *Nature*, 2000, (406), pp. 188–192
- [18] Asthagiri, A. R., and Lauffenburger, D. A.: ‘A computational study of feedback effects on signal dynamics in a mitogen-activated protein kinase (MAPK) pathway model’, *Biotechnol. Prog.*, 2001, **17**, pp. 227–239
- [19] Meinhardt, H., and de Boer, P. A.: ‘Pattern formation in *Escherichia coli*: a model for the pole-to-pole

- oscillation of MIN proteins and the localization of the division site', *Proc. Natl. Acad. Sci. USA*, 2001, **98**, pp. 14202-7
- [20] Chen, K. C., Calzone, L., Csikasz-Nagy, A., Cross, F. R., Novak, B., and Tyson, J. J.: 'Integrative Analysis of Cell Cycle Control in Budding Yeast', *Mol. Biol. Cell*, 2004, **15**, (8), pp. 3841-3862
- [21] Cross, F. R., Archambault, V., Miller, M., and Klovstad, M.: 'Testing a Mathematical Model of the Yeast Cell Cycle', *Mol. Biol. Cell*, 2002, **13**, (1), pp. 52-70
- [22] Hoffmann, A., Levchenko, A., Scott, M. L., and Baltimore, D.: 'The I κ B-NF- κ B Signaling Module: Temporal Control and Selective Gene Activation', *Science*, 2002, **298**, (5596), pp. 1241-1245
- [23] Pomerening, J. R., Sontag, E. D., and Ferrell, J. E. Jr.: 'Building a cell cycle oscillator: hysteresis and bistability in the activation of Cdc2', *Nature Cell Biology*, 2003, **5**, pp. 346-351
- [24] Sha, W., Moore, J., Chen, K., Lassaletta, A. D., Yi, C., Tyson, J. J., and Sible, J. C.: 'Hysteresis drives cell-cycle transitions in *Xenopus laevis* egg extracts', *PNAS*, 2003, **100**, (3), pp. 975-980
- [25] Eissing, T., Conzelmann, H., Gilles, E. D., Allgöwer, F., Bullinger, E., and Scheurich, P.: 'Bistability analyses of a caspase activation model for receptor-induced apoptosis', *J. Biol. Chem.*, 2004, **279**, (35), pp. 36892-36897
- [26] Barkai, N., and Leibler, S.: 'Robustness in simple biochemical networks', *Nature*, 1997, (387), pp. 913-917
- [27] Zwolak, J.W., Tyson, J.J., and Watson, L.T.: 'Parameter Estimation for a Mathematical Model of the Cell Cycle in Frog Eggs', *Journal of Computational Biology*, 2004, to appear
- [28] Marlovits, G., Tyson, C.J., Novak, B., and Tyson, J.J.: 'Modeling M-phase control in *Xenopus* oocyte extracts: the surveillance mechanism for unreplicated DNA', *Biophys. Chem.*, 1998, **72**, pp. 169-184
- [29] Novak, B. and Tyson, J.: 'Numerical Analysis of a Comprehensive Model of M-phase Control in *Xenopus* Oocyte Extracts and Intact Embryos', *Journal of Cell Science*, 1993, **106**, pp. 1153-68
- [30] Kumagai, A., and Dunphy, W. G.: 'Regulation of the cdc25 Protein during the Cell Cycle in *Xenopus* Extracts', *Cell*, 1992, **70**, pp. 139-151
- [31] Kumagai, A., and Dunphy, W. G.: 'Control of the Cdc2/Cyclin B Complex in *Xenopus* Egg Extracts Arrested at a G2/M Checkpoint with DNA Synthesis Inhibitors', *Mol. Bio. of the Cell*, 1995, **6**, pp. 199-213
- [32] Tang, Z., Coleman, T. R., and Dunphy, W. G.: 'Two distinct mechanisms for negative regulation of the Wee1 protein kinase', *EMBO J.*, 1993, **12**, (9), pp. 3427-36
- [33] Solomon, M. J., Glotzer, M., Lee, T. H., Philippe, M., and Kirschner, M. W.: 'Cyclin Activation of P34cdc2', *Cell*, 1990, **63**, pp. 1013-1024
- [34] Dennis, J. E. Jr., and Schnabel, R. B.: 'Numerical Methods for Unconstrained Optimization and Non-linear Equations', (Prentice-Hall, Inc., Englewood Cliffs, NJ 1983)
- [35] Moore, J.: Private Communication, Aug 1997
- [36] He, J., Watson, L.T., Ramakrishnan, N., Shaffer, C.A., Verstak, A., Jiang, J., Bae, K., and Tranter, W.H.: 'Dynamic data structures for a direct search algorithm', *Comput. Optim. Appl.*, 2002, **23**, pp. 5-25
- [37] Boggs, P. T, Donaldson, J. R., Byrd, R. H., and Schnabel, R. B.: 'ALGORITHM 676 ODRPACK: Software for Weighted Orthogonal Distance Regression', *ACM Trans. on Math. Soft.* 15, 1989, **4**, pp. 348-364
- [38] Hindmarsh, A.C.: 'LSODE and LSODI, Two New Initial Value Ordinary Differential Equation Solvers', *ACM SIGNUM Newsletter* 15, 1980, **4**, pp. 10-11
- [39] He, J., Verstak, A., Watson, L.T., Stinson, C.A., Ramakrishnan, N., Shaffer, C.A., Rappaport, T.S., Anderson, C.R., Bae, K., Jiang, J., and Tranter, W.H.: 'Globally optimal transmitter placement for indoor wireless communication systems', *IEEE Trans. Wireless Commun.*, 2004, **3**, pp. ?-?
- [40] Watson, L.T., Baker, C.A.: 'A fully-distributed parallel global search algorithm', *Engrg. Comput.*, 2001, **18**, pp. 155-169
- [41] Jones, D.R., Perttunen, C.D., and Stuckman, B.E.: 'Lipschitzian Optimization Without the Lipschitz Constant', *Journal of Optimization Theory and Applications*, 1993, **79**, (1), pp. 157-181
- [42] Boggs, P.T., Byrd, R.H., Rogers, J.E., and Schnabel, R.B.: 'User's Reference Guide for ODRPACK Version 2.01: Software for Weighted Orthogonal Distance Regression', (Center for Computing and Applied Mathematics, U.S. Department of Commerce, Gaithersburg, MD, 1992)

- [43] Boggs, P.T., Byrd, R.H., and Schnabel, R.B.: ‘A Stable and Efficient Algorithm for Nonlinear Orthogonal Distance Regression’, *SIAM J. Sci. Stat. Comput.* 8, 1987, **6**, pp. 1052–78
- [44] Radhakrishnan, K., and Hindmarsh, A.C.: ‘Description and Use of LSODE, the Livermore Solver for Ordinary Differential Equations’, (NASA Reference Publication 1327. Lawrence Livermore National Laboratory Livermore, CA, Dec 1993)
- [45] Hindmarsh, A.C.: ‘ODEPACK: A Systematized Collection of ODE Solvers, 55–64’, Stepleman, R.S., et al., eds., Scientific Computing, 1983, (North Holland Publishing Co. New York)
- [46] Petzold, L.: ‘Automatic Selection of Methods for Solving Stiff and Nonstiff Systems of Ordinary Differential Equations’, *SIAM Journal on Scientific and Statistical Computing*, 1983, **4**, pp. 136–148
- [47] Shampine, L.F., and Allen, R.C.: ‘Numerical Computing: An Introduction’, (W. B. Saunders Company Philadelphia, PA, 1973)
- [48] Dekker, T.J.: ‘Finding a zero by means of successive linear interpolation’, Dejon, B., and Henrici, P., eds., Constructive Aspects of the Fundamental Theorem of Algebra, 1969, (Wiley-Interscience London)